Materials science / Материаловедение

UDC 621.78.084:620.186
DOI 10.17073/0368-0797-2024-2-195-204

Original article
Оригинальная статья

Effect of heat treatment modes on structure and properties of 08Kh18N6AG10S steel

A. I. Gordienko[1], E. V. Abdulmenova[1], T. V. Kozlova[1], Yu. F. Gomorova[1], I. V. Vlasov[1], I. A. Fotin[1], K. N. Kayurov[2], S. P. Buyakova[1]

[1] **Institute of Strength Physics and Materials Science, Siberian Branch of Russian Academy of Sciences** (2/4 Akademicheskii Ave., Tomsk 634055, Russian Federation)
[2] **LLK Scientific Production Enterprise of Geophysical Equipment "Luch"** (49 Geological str., Novosibirsk 630010, Russian Federation)

mirantil@ispms.ru

Abstract. The paper studies the influence of heat treatment modes on the structure and properties of austenitic steel grade 08Kh18N6AG10S. Austenitic structure with twinned boundaries was preserved after quenching at 1040 and 1100 °C. At the same time, the average size of austenitic grains decreased from 42.3 ± 6 μm (supply condition) to 38.1 ± 5.0 and 39.0 ± 4.5 μm, respectively. Quenching at 1040 °C leads to release of excess carbide phases at the grain boundaries. Mainly manganese and silicon oxides were found after quenching at 1100 °C. Quenching at 1040 °C leads to a slight decrease in microhardness (by 12 %) compared to the condition of supply (from 3285 ± 80 to 2895 ± 70 MPa). The hardness decreases less after quenching at 1100 °C (up to 3090 ± 80 MPa). Quenching at 1040 and 1100 °C has significantly improved the fracture toughness of steel. Values of impact strength of the steel increased to 223 ± 10 and 240 ± 5 J/cm^2 compared to the condition of supply (55 J/cm^2). The authors found that the steel samples demonstrate a comparable level of wear resistance during tests for abrasive wear compared to the condition of supply after quenching at 1040 and 1100 °C. The mass loss after passing the roller distance of 4309 m for all steel conditions is approximately 8.0 %. The authors concluded that the most optimal heat treatment of 08Kh18N6AG10S steel is quenching at 1100 °C, which improves the fracture toughness of steel while maintaining microhardness and wear resistance.

Keywords: non-magnetic austenitic steel, hardening, microstructure, phase composition, fracture toughness, microhardness, abrasive wear

Acknowledgements: The work was performed within the framework of the state task of the Institute of Strength Physics and Materials Science, Siberian Branch of Russian Academy of Sciences, project No. FWRW-2021-0009. The authors express their gratitude to V.N. Eremin for providing material for research, I.N. Sevostyanova for assistance in preparing samples for microstructural studies and mechanical tests, A.A. Neumann for conducting structural studies using scanning electron microscopy, V.V. Shmakov for assistance in conducting abrasive tests.

For citation: Gordienko A.I., Abdulmenova E.V., Kozlova T.V., Gomorova Yu.F., Vlasov I.V., Fotin I.A., Kayurov K.N., Buyakova S.P. Effect of heat treatment modes on structure and properties of 08Kh18N6AG10S steel. *Izvestiya. Ferrous Metallurgy*. 2024;67(2):195–204.
https://doi.org/10.17073/0368-0797-2024-2-195-204

Влияние режимов термической обработки на структуру и свойства стали 08Х18Н6АГ10С

А. И. Гордиенко[1], Е. В. Абдульменова[1], Т. В. Козлова[1], Ю. Ф. Гоморова[1], И. В. Власов[1], И. А. Фотин[1], К. Н. Каюров[2], С. П. Буякова[1]

[1] **Институт физики прочности и материаловедения Сибирского отделения РАН** (Россия, 634055, Томск, пр. Академический, 2/4)
[2] **ООО Научно-производственное предприятие геофизической аппаратуры «Луч»** (Россия, 630010, Новосибирск, ул. Геологическая, 49)

mirantil@ispms.ru

Аннотация. Исследовано влияние режимов термической обработки на структуру и свойства аустенитной стали марки 08Х18Н6АГ10С. После закалки от 1040 и 1100 °С сохранилась аустенитная структура с двойникованными границами, при этом произошло уменьшение среднего размера аустенитных зерен с 42,3 ± 6 мкм (состояние поставки) до 38,1 ± 5,0 и 39,0 ± 4,5 мкм соответственно. После закалки от 1040 °С происходит выделение избыточных карбидных фаз на границах зерен. После закалки от 1100 °С обнаружены преимущественно оксиды марганца и кремния. Закалка стали от температуры 1040 °С приводит к незначительному снижению микротвердости (на 12 %) по сравнению с состоянием поставки (с 3285 ± 80 до 2895 ± 70 МПа). После закалки от 1100 °С твердость снижается в меньшей степени (до 3090 ± 80 МПа). Проведение закалки от 1040 и 1100 °С позволило существенно улучшить ударную вязкость разрушения стали. Значения ударной вязкости стали возросли до 223 ± 10 и 240 ± 5 Дж/см^2 по сравнению с состоянием поставки (55 Дж/см^2). При проведении испытаний на абразивный износ обнаружено, что образцы стали после закалки от 1040 и 1100 °С демонстрируют сопоставимый уровень износостойкости по сравнению с состоянием поставки. Потеря массы после прохождения дистанции ролика 4309 м для всех состояний стали составляет примерно 8,0 %. Сделано заключение, что оптимальной термической обработкой стали марки 08Х18Н6АГ10С является закалка от температуры 1100 °С, которая позволяет улучшить вязкость разрушения стали при сохранении микротвердости и износостойкости.

Ключевые слова: немагнитная аустенитная сталь, закалка, микроструктура, фазовый состав, ударная вязкость разрушения, микротвердость, абразивный износ

Благодарности: Работа выполнена в рамках государственного задания Института физики прочности и материаловедения Сибирского отделения РАН, тема номер FWRW-2021-0009. Авторы благодарят В.Н. Еремина за предоставление материала для исследований, И.Н. Севостьянову за помощь в подготовке образцов для микроструктурных исследований и механических испытаний, А.А. Неймана за проведение структурных исследований с помощью растровой электронной микроскопии, В.В. Шмакова за помощь в проведении абразивных испытаний.

Для цитирования: Гордиенко А.И., Абдульменова Е.В., Козлова Т.В., Гоморова Ю.Ф., Власов И.В., Фотин И.А., Каюров К.Н., Буякова С.П. Влияние режимов термической обработки на структуру и свойства стали 08Х18Н6АГ10С. *Известия вузов. Черная металлургия*. 2024;67(2):195–204. https://doi.org/10.17073/0368-0797-2024-2-195-204

Introduction

In recent years, oil-producing companies have shown increased interest in fields with hard-to-recover (HTR) oil reserves. According to 2021 statistics, extraction from hard-to-recover oil reserves accounts for about 44 % of produced oil, and approximately 25 % of gas is extracted from HTR natural gas reserves [1; 2]. Modern directionally drilling technology – rotary steerable systems (RSS) – is used to develop HTR oil reserves with both horizontally and directionally well profiles [3; 4].

The RSS operates in direct contact with the aggressive liquid medium of the drilling agent, which contains salt solutions and a suspension of silicate sand particles, leading to accelerated corrosion and water-abrasive wear of the RSS components. Recesses were made in the RSS housing on the outer surface to accommodate telemetry and gamma-ray logging systems for carrying out geophysical research during drilling [5]. For stable and reliable RSS operation, its components must be made of non-magnetic, corrosion-resistant materials with high hardness and resistance to water-abrasive wear.

The most suitable materials for manufacturing RSS components are non-magnetic austenitic steels since their high strength, corrosion resistance, and significant wear resistance [6]. It was noted in [7] that steels with a high chromium content successfully combine strength, wear resistance, fracture toughness and creep resistance. Therefore, it is advisable to use them in conditions of increased abrasion. The study [8] revealed that steels containing 25 wt. % Mn are exceptionally ductile and strong as deformation twins form at room temperature [9; 10]. Joint alloying with nickel and chromium increases the ductility and fracture toughness of steel. Obtained steels, for example, 08Kh18N10, 02Kh18N11, 12Kh18N10T are well processed by cold and hot deformation. To enhance the performance of these steels at temperatures above 450 °C, they are additionally alloyed with nitrogen [11 – 13], which improves their strength properties. At the same time, the plastic properties of nitrogen-containing steels are rather high [3; 14]. Nitrogen is a strong austenite-forming element; it replaces expensive nickel and manganese and reduces magnetic permeability [4; 11]. Alloying austenitic steels with nitrogen enhances their resistance to local corrosion [5; 12]. The physical and mechanical properties of steels alloyed with nitrogen improve due to the precipitation of fine and homogeneously distributed chromium and vanadium nitrides instead of coarser carbide precipitates [15]. Alloying with nitrogen leads to structural and phase transformations in steel which significantly affect the mechanical properties [16; 17].

Based on the above, the non-magnetic 08Kh18N6AG10S steel alloyed with chromium, nickel, manganese, and nitrogen can be selected as RSS housing elements material. Complex steel alloying should ensure the RSS operation in an aggressive environment.

Complex steel alloying should ensure the RSS operation in an aggressive environment. To obtain optimal mechanical characteristics required for the material operating in aggressive environments, austenitic nitrogen steels are subjected to thermal and thermomechanical treatments [18]. Heat treatment of chromium-nickel and chromium-manganese-nickel austenitic steels involves quenching in water at temperatures from 1050 to 1100 °C. Heating to the temperatures should ensure the chromium carbides dissolution, while rapid cooling should maintain the supersaturated solid solution state. Despite numerous publications on the heat treatment effect on the nitrogen austenitic steel structure, phase composition, and mechanical properties, information on the 08Kh18N6AG10S steel used for the RSS protective components is rather limited.

The purpose of the work is to study the impact of heat treatment modes on the structure, phase composition, and mechanical properties of 08Kh18N6AG10S steel.

Materials and methods

The industrial 08Kh18N6AG10S steel in as-forged (condition of supply) with the following chemical composition, wt. %: C < 0.06, 8.5 – 10.0 Mn, 0.6 – 1.2 Si, P < 0.03, S < 0.03, 16.0 – 18.0 Cr, 5.0 – 6.0 Ni, Al < 0.02, 0.01 – 0.02 Ca, N > 0.4 and Fe-rest, was investigated. The steel was heat treated in a SNOL 185/1200 electric chamber furnace in an argon atmosphere at temperatures of 1040 and 1100 °C for 40 min, followed by quenching in water. For structural studies, samples were cut by electrical discharge machining into rectangular plates with dimensions of 10×10×3 mm.

The sample surfaces were ground on abrasive paper with a gradual reduction in abrasive grain size and polished with diamond pastes of varying dispersion. Grain boundaries were etched with a solution of nitric (HNO_3) and hydrochloric (HCl) acids in a volume ratio of 25:75. Microstructural studies were conducting using an Altami MET 1M optical microscope and a scanning electron microscope (SEM) (LEO EVO 50) equipped with an energy-dispersive spectrometer.

Methods of *X*-ray phase and *X*-ray diffraction analysis were employed to determine the fine crystal structure (size of the coherent scattering region (CSR), lattice parameter), and phase composition of the steel. *X*-ray diffraction patterns were obtained using a diffractometer with filtered CuK_α radiation. The *X*-ray was performed in the angle range from 40 to 120° with a step of 0.05° and exposure for each point was set to ensure a statistical accuracy of a minimum of 0.5 %. Phases were identified by comparing the peaks of the *X*-ray diffraction patterns with the PDF-2 ICDD structural database. The parameters of the crystal cells were determined based on the interplanar distances (*d*) for all reflections in the angle range from 40 to 120°. The full width at half maximum (FWHM) of the *X*-ray lines was determined by approximating the diffraction lines using the Lorentz function. The coherent scattering region was calculated using the Scherrer equation [19] for the most intense lines of the *X*-ray spectra. Microstresses of 08Kh18N6AG10S steel were assessed according to the *X*-ray data based on [20], using calculated microdistortions and literature data on Young's modulus. The microdistortion was determined using the Stokes–Wilson equation [21]. Microstresses in the γ-Fe phase were calculated based on the last most distinguishable diffraction reflection with a plane index (222) under the assumption that microdistortion is the main factor determining the diffraction width at far angles.

Steel microhardness was measured using the Vickers method on a PMT-3 at a load of 0.98 N and using the Rockwell method on a TK-″M N1916 at a load of 98.7 N. Samples of 10×10×55 mm *V*-shaped notched of IX type according to GOST 6996 – 66 underwent impact bending tests at room temperature using a KM-300-M-Sh pendulum impact testing machine. Macroimages of destroyed samples were received using an Altami SM0870 stereographic microscope. Fracture micromechanisms were studied using a LEO EVO 50 scanning electron microscope.

The samples were subjected to abrasive wear tests according to the ASTM G65-04 standard [22]. Plates were fixed in the holder of the abrasive wear unit, oriented so that the rubber roller touched the sample at its center. Quartz sand with a fraction size of 200 – 300 μm was supplied to the point of contact of the sample with a rubber roller at a speed of 400 g/min. The roller rotation speed was 100 rpm. Tests were conducted following method D of the ASTM G65-04 standard, wherein the roller distance was 4309 m, and the roller clamping force was 45 N. After completion of the test, as well as at intervals of linear continuous contact between the sample and the roller of 1000, 2000, 3000, and 4309 m, the samples were removed from the holder and weighed on an analytical laboratory balance AV-120-01 with an accuracy of 0.0001 g, followed by the relative weight loss control.

Results and discussion

Microstructural studies

Fig. 1 illustrates the microstructures of 08Kh18N6AG10S steel in the supply conditions and after quenching at 1040 and 1100 °C. The steel structure in the supply conditions features large austenitic grains (Fig. 1, *a*) with an average size of 42.3 ± 6 μm with a large number of twins characterized for austenite (Fig. 1, *a*, indicated by arrows) [23]. Quenching at temperature of 1040 and 1100 °C resulted in grain refinement, the average grain size reduced to 38.1 ± 5.0 μm and 39 ± 4.5 μm, respectively (Fig. 1, *b*, *c*). The reduction in grain size is likely due to the high cooling rate during quenching. The austenitic structure with twin boundaries remains intact. Additionally, dark areas were observed at the boundaries of austenite grains in the microstructure after quenching at 1040 °C (Fig. 1, *d*). Higher magnification revealed numerous inclusions within the dark areas of the grain boundaries (inset in the bottom corner, Fig. 1, *d*). Energy dispersive analysis during SEM enabled the detection of carbon segregations in the boundary regions (inset in the upper corner, Fig. 1, *d*). This phenomenon is attributed to incomplete dissolution of all alloying elements during heating to 1040 °C, leading to carbide precipitation at grain boundaries. During rapid cooling, particle segregation at grain boundaries can result in microcracks. These particle segregations and microcracks in steel after quenching at 1040 °C are considered as structural defects that can affect the properties of the steel. The authors [13]

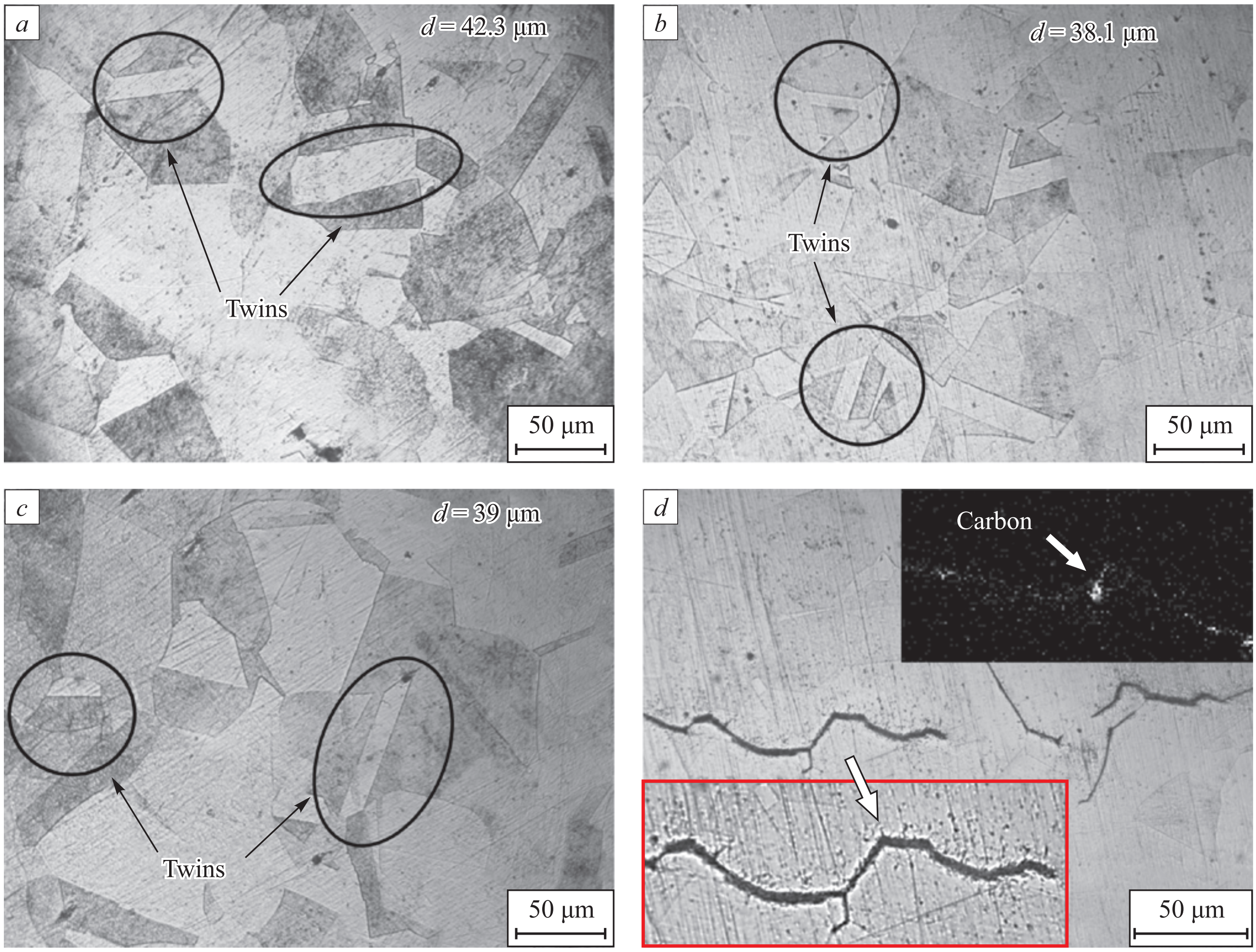

Fig. 1. Microstructure of 08Kh18N6AG10S steel in condition of supply (*a*), after quenching at 1040 °C (*b*, *d*) and 1100 °C (*c*)

Рис. 1. Микроструктура стали марки 08Х18Н6АГ10С в состоянии поставки (*а*), после закалки от 1040 °C (*b*, *d*) и от 1100 °C (*c*)

noted that as carbide phases precipitated along grain boundaries, the susceptibility to intergranular corrosion of steel increased.

Fig. 2 presents the *X*-ray diffraction patterns of 08Kh18N6AG10S steel in the condition of supply and after quenching at 1040 and 1100 °C. All *X*-ray diffraction patterns exhibit lines corresponding to the γ-Fe phase with a face-centered cubic lattice. Quenching of the steel resulted in a decrease in the full width at half maximum (FWHM) of the γ-Fe phase diffraction lines compared to the *X*-ray diffraction pattern of the steel in the condition of supply. For instance, the FWHM of the diffraction reflection (111) decreased from 0.2496 to 0.1797° at a quenching temperature of 1040 °C and from 0.2496 to 0.2080° at a quenching temperature of 1100 °C. This trend aligns with the findings of [24], where heat treatment of Fe – Cr – Mn – C – N steel resulted in a decrease in FWHM of diffraction lines from 1.1 to 0.89°. The reduction in FWHM of diffraction lines may stem from an

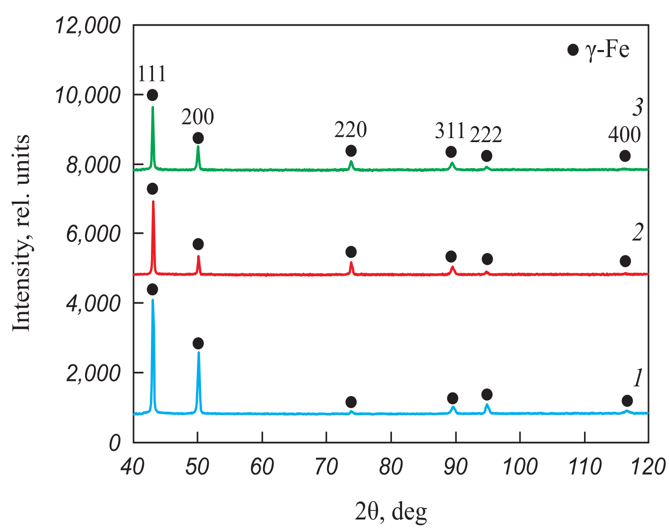

Fig. 2. *X*-ray images of 08Kh18N6AG10S steel in condition of supply (*1*), after quenching at 1040 °C (*2*) and 1100 °C (*3*)

Рис. 2. Рентгенограммы стали марки 08Х18Н6АГ10С в состоянии поставки (*1*), после закалки от 1040 °C (*2*) и 1100 °C (*3*) increased size of coherent scattering regions and changes in microstress values due to quenching.

The *X*-ray diffraction patterns of all studied conditions show no lines characteristic of free carbon or carbides (Fig. 2), indicating that the proportion of the carbide phase is insignificant relative to the austenitic matrix.

The cell parameter of the γ-Fe phase of steel in the condition of supply was measured at $0.3629 \pm 5 \cdot 10^{-4}$ nm. After quenching the cell parameter of the γ-Fe phase changed insignificantly to $0.3631 \pm 5 \cdot 10^{-4}$ nm after quenching at 1040 °C and $0.3633 \pm 5 \cdot 10^{-4}$ nm after quenching at 1100 °C.

Calculation of type II stresses revealed that after quenching at 1040 °C, microstresses present in the initial steel structure relaxed. Type II stresses decreased from 0.27 GPa in the supply condition to 0.24 GPa after quenching at 1040 °C. Quenching at 1100 °C leaded to the microstress value increased to 0.32 GPa, likely due to the formation of a fine-grained structure and better dissolution of alloying components in the solid solution.

Mechanical properties of steel

Table 1 displays the microhardness values and the results of impact tests for steel 08Kh18N6AG10S conducted at room temperature. The microhardness of the steel in the condition of supply was 3285 ± 80 MPa, which aligns well with literature data [25]. After quenching the microhardness decreased to 2895 ± 70 MPa (equivalent to 30 ± 1 HRC) at 1040 °C and to 3090 ± 80 MPa (equivalent to 32 ± 1 HRC) at 1100 °C. Notably, the microhardness values of steel after quenching at 1040 °C are lower compared to those after quenching at 1100 °C. This suggests that the heating temperature of 1040 °C may not be sufficient for all alloying elements to enter the solid solution, leading to carbide precipitation at grain boundaries (Fig. 1, *d*). Consequently, the effect of solid solution hardening is more pronounced in steel after quenching at 1100 °C. This aligns with the type II stresses calculation results, showing an increase in microstress to 0.32 GPa after quenching at 1100 °C.

The hardness of chromium-manganese-nickel austenitic steels decreases during quenching as carbides of alloying elements dissolve and the supersaturated solid solution is maintained during rapid cooling. Additionally, recrystallization processes during quenching eliminate the effect of dislocation hardening due to plastic deformation under forging.

The fracture toughness of steel in the condition of supply is 55 J/cm^2. Fractures of the steel samples in the condition of supply exhibit minimal tightening of the side faces, and shear lips are practically absent (Fig. 3, *a*), indicating that macroplastic deformation preceding destruction is not significant.

The fracture micromechanism of steel in the condition of supply is mixed, featuring large pits characteristic of ductile fracture, as well as areas of brittle fracture with typical cleavage facets and microcracks (Fig. 3, *a*, inset). Cracking is observed within large austenite grains. Energy dispersive analysis revealed that second-phase inclusions in large pits consist of manganese and iron carbides, silicon, and aluminum oxides (Table 2, with areas of energy dispersive analysis indicated in Fig. 3 as an example). The size of round particles ranges from 3.2 to 5.0 µm.

After quenching at 1040 °C, the fracture toughness of the steel is significantly higher (Table 1) compared to the condition of supply. Concurrently, the tightening of the side faces and the width of the shear lip areas at the fractures (Fig. 3, *b*, marked with an arrow), which characterize the degree of plastic deformation as the crack develops, increased. The destruction micromechanism of the samples is entirely ductile and dimple-shaped, without signs of brittle fracture (Fig. 3, *b*, inset).

Round and elongated particles, with shapes close to plates, were detected in the pits. The size of round particles ranged from 1.5 to 5.5 µm, while the size of elongated particles reached 3×15 µm.

After quenching at 1100 °C, the impact strength of the steel is the highest among those presented, reaching 240 ± 5 J/cm^2 (Table 1). The fractures of the samples are characterized by a high degree of tightening (Fig. 3, *c*, marked with an arrow) and sophisticated surface topogra-

Table 1. **Microhardness and results of impact tests of 08Kh18N6AG10S steel at room temperature**

Таблица 1. **Микротвердость и результаты ударных испытаний, проведенных при комнатной температуре, стали марки 08Х18Н6АГ10С**

Steel condition	Hardness		Fracture toughness, J/cm^2	Fracture energy, J
	according to Vickers, MPa	HRC		
Supply	3285 ± 80	35 ± 1	55 ± 11	44 ± 11
Quenching at 1040 °C	2895 ± 70	30 ± 1	223 ± 10	178 ± 10
Quenching at 1100 °C	3090 ± 80	32 ± 1	240 ± 5	192 ± 5

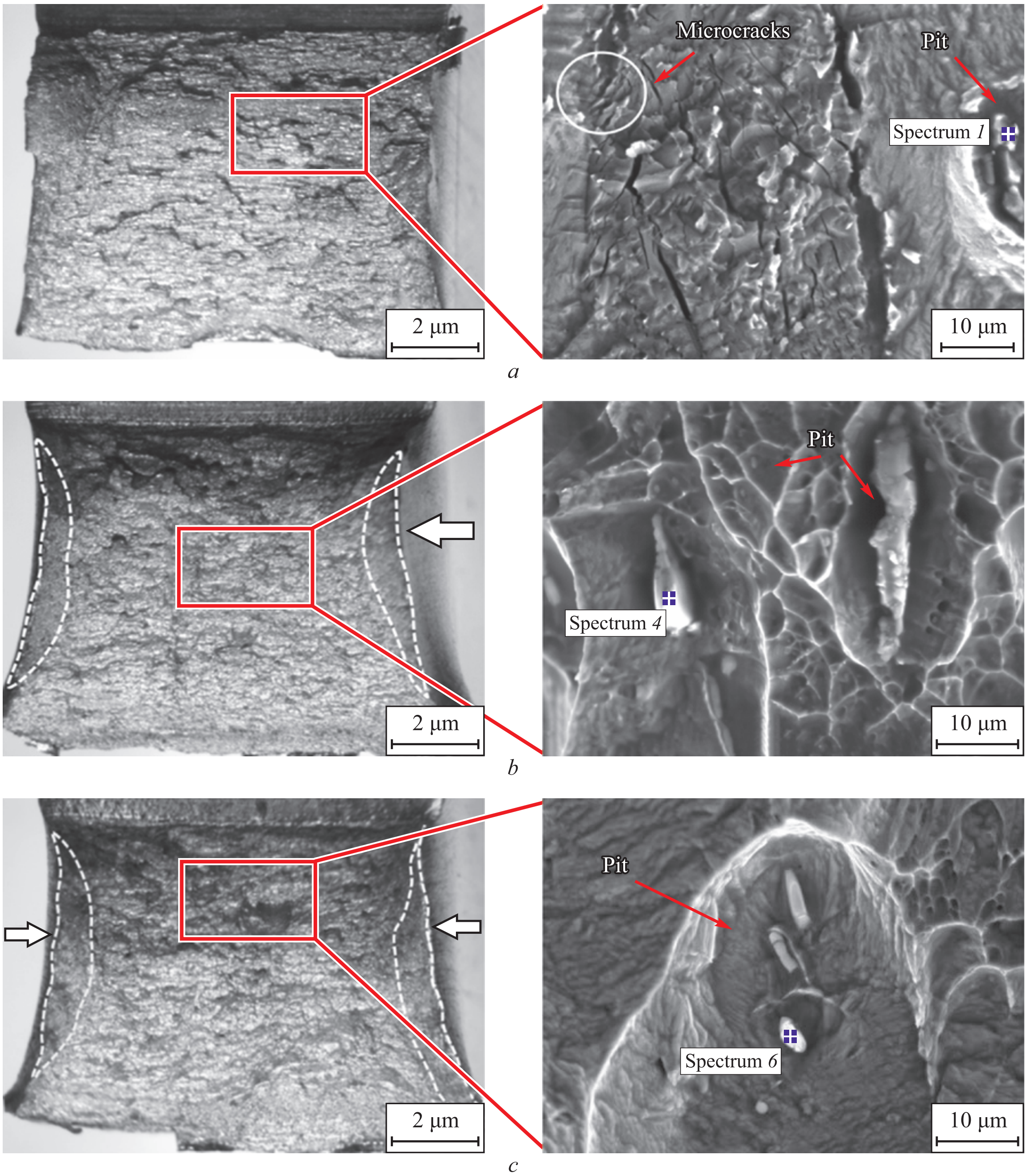

Fig. 3. Fracture surfaces of 08Kh18N6AG10S steel in condition of supply (*a*), after quenching at 1040 °C (*b*) and 1100 °C (*c*)

Рис. 3. Поверхности разрушения стали марки 08Х18Н6АГ10С в состоянии поставки (*a*), после закалки от 1040 °C (*b*) и 1100 °C (*c*)

phy. Large pores on the fracture surface indicate the ductile nature of the fracture. Particles of different morphologies and sizes were found in the pores (Fig. 3, *c*). These include round particles, ranging in size from 3.5 to 5.0 μm, dispersed particles with sizes of 0.8 – 1.5 μm, and elongated particles measuring 1.5 × 7.0 μm. According to the energy dispersive analysis data, the particles in the pits are primarily oxides of manganese and silicon (Table 2). The proportion of carbide inclusions in the steel after quenching at 1100 °C is significantly smaller. This confirms the earlier conclusions that when heated to 1100 °C, most of the alloying elements enter the solid solution, leading to a reduction in the carbide inclusions of in the steel. The smaller proportion of carbide particles and their smaller size account for the higher fracture toughness of the steel in this structural condition (Table 1).

During the abrasive wear testing of the steel in different structural conditions, marked traces of abrasive wear and changes in the geometry of the samples are observed after the roller covers a distance of 4309 m (the traces of abrasive wear of the sample in the supply condition are shown as an example, Fig. 4, *a*).

Table 2. **Result of *X*-ray energy dispersive microanalysis obtained from fractures of 08Kh18N6AG10S steel**

Таблица 2. **Результаты энергодисперсионного микроанализа, полученные с изломов стали марки 08Х18Н6АГ10С**

Spectrum	Element content, at. %							
	C	O	Mg	Al	Si	Cr	Mn	Fe
Supply condition								
Spectrum *1*	45.1	–	–	–	–	4.6	42.3	8.0
Spectrum *2*	14.9	46.0	8.5	21.5	–	3.8	4.1	1.2
Quenching at 1040 °C								
Spectrum *3*	50.7	–	–	–	0.5	1.2	46.0	1.6
Spectrum *4*	19.3	46.5	5.6	–	11.9	0.6	15.2	0.9
Quenching at 1100 °C								
Spectrum *5*	7.9	51.9	8.6	–	13.9	0.8	15.7	1.2
Spectrum *6*	15.5	49.5	2.0	–	11.1	1.8	17.0	3.1

In all three cases, the maximum decrease in the sample height is approximately 1.5 mm and observed at the center, corresponding to 15 % of the total sample height. Fig. 4, *b* depicts the dependence of mass loss on the roller path during the testing of 08Kh18N6AG10S steel. The dependencies for all samples are linear. Steels in the condition of supply and after quenching at 1040 °C exhibit comparable weight loss values, approximately 7.7 %. After quenching at 1100 °C, the weight loss is slightly greater about 8.5 %. It can be concluded that quenching and changes in the structural condition of the steel do not significantly alter the wear resistance.

Thus, when 08Kh18N6AG10S steel is utilized to manufacture the RSS housing, quenching at 1100 °C is recommended. Suggested heat treatment can notably enhance the fracture toughness of the steel without compromising wear resistance and hardness. Additionally, quenching at a temperature of 1100 °C results in a decrease in the proportion of carbide inclusions with magnetic properties, which are unacceptable when conducting geophysical research during drilling.

Conclusions

After quenching 08Kh18N6AG10S steel at 1040 and 1100 °C, an austenitic structure forms with grain sizes of 38.1 ± 5.0 and 39 ± 4.5 μm, respectively. It was observed that quenching at 1040 °C leads to the precipitation of excess carbide phases at grain boundaries due to incomplete austenitization.

According to energy dispersive analysis, the proportion of carbide inclusions decreases after quenching at 1100 °C with the main inclusions being manganese and silicon oxides.

The research revealed that quenching at 1040 and 1100 °C significantly increases the fracture toughness of 08Kh18N6AG10S steel to 223 – 240 J/cm^2 compared to the condition of supply values of 55 J/cm^2.

Abrasive wear tests demonstrated that despite decreased hardness and increased fracture toughness steel samples after quenching at 1040 and 1100 °C exhibit approximately the same wear resistance as the as-supplied steel.

Therefore, we recommend quenching at 1100 °C for 08Kh18N6AG10S steel used in RSS housing manufacturing as it provides the required mechanical properties and helps to reduce the proportion of magnetic inclusions in the material.

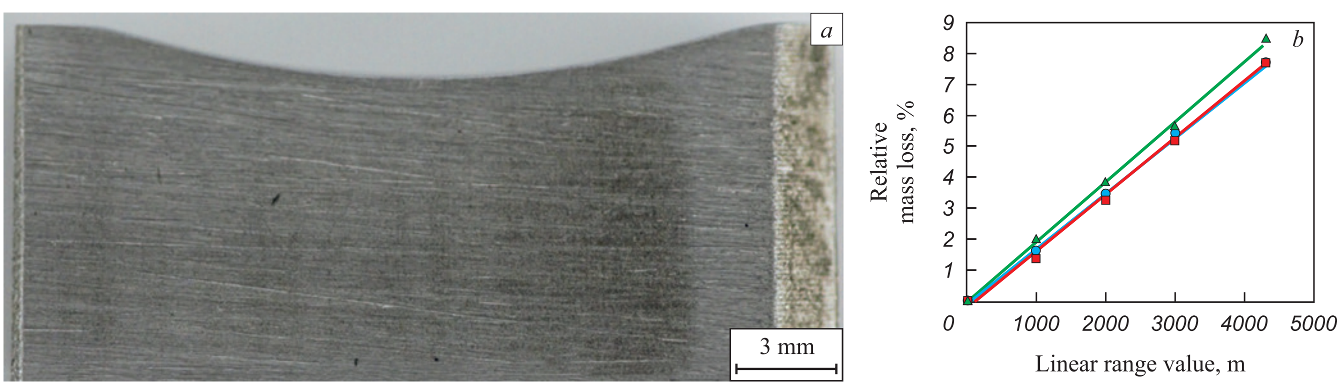

Fig. 4. Macrophotograph of lateral side of the steel sample in condition of supply after passing the distance from the roller of 4309 m (*a*), dependences of the mass loss on the roller path during abrasive wear tests 08Kh18N6AG10S steel (*b*):
● – in condition of supply; ■ and ▲ – after quenching at 1040 and 1100 °C

Рис. 4. Макрофотография боковой стороны образца стали в состоянии поставки после прохождения дистанции ролика 4309 м (*a*), зависимость потери массы от пути ролика при испытаниях на абразивный износ стали марки 08Х18Н6АГ10С (*b*):
● – в состоянии поставки; ■ и ▲ – после закалки от 1040 и 1100 °C

References / Список литературы

1. Brook B.W., Alonso A., Meneley D.A., Misak J., Blees T., van Erp J.B. Why nuclear energy is sustainable and has to be part of the energy mix. *Sustainable Materials and Technologies*. 2014;1-2:8–16. https://doi.org/10.1016/j.susmat.2014.11.001
2. Jia C., Pang X., Song Y. The mechanism of unconventional hydrocarbon formation: Hydrocarbon self-sealing and intermolecular forces. *Petroleum Exploration and Development*. 2021;48(3):507–526. https://doi.org/10.1016/s1876-3804(21)60042-3
3. Shevchenko I.A. Drilling wells with a large departure from the vertical, using a rotary-driven systems with control geophysical parameters in real-time. *Modern Science: Actual Problems of Pheory and practice. Series: Natural and Technical Sciences*. 2014;(1-2):36–39. (In Russ.).

   Шевченко И.А. Бурение скважин с большим отходом от вертикали с использованием роторных управляемых систем при контроле геофизических параметров в режиме реального времени. *Современная наука: актуальные проблемы теории и практики. Серия: естественные и технические науки*. 2014;(1-0):36–39.
4. Zakirov A.Ya. The first test results of Russian-made rotary-controlled systems. *Proneft'. Professionally about oil*. 2016;(2(2)):43–47. (In Russ.).

   Закиров А.Я. Первые результаты испытаний роторно-управляемых систем российского производства. *Pro-нефть. Профессионально о нефти*. 2016;(2(2)):43–47.
5. Zhang C., Zou W., Cheng N. Overview of rotary steerable system and its control methods. In: *Proceedings of 2016 IEEE Int. Conf. on Mechatronics and Automation*. 2016: 1559–1565. https://doi.org/10.1109/icma.2016.7558796
6. Kushnereva D.S., Sapozhnikov G.V. Properties investigations of the new high-strength stainless steels. *Chemical Physics and Mesoscopy*. 2019;21(1):39–44. (In Russ.). https://doi.org/10.15350/17270529.2019.1.6

   Кушнерева Д.С., Сапожников Г.В. Исследование свойств новых высокопрочных нержавеющих сталей. *Химическая физика и мезоскопия*. 2019;21(1):39–44. https://doi.org/10.15350/17270529.2019.1.6
7. Foldyna V., Kubon Z., Filip M., Mayer K.-H., Berger C. Evaluation of structural stability and creep resistance of 9–12 % Cr steels. *Steel Research*. 1996;67(9):375–381. https://doi.org/10.1002/srin.199605504
8. Grässel O., Krüger L., Frommeyer G., Meyer L.W. High strength Fe–Mn–(Al, Si) TRIP/TWIP steels development – properties – application. *International Journal of Plasticity*. 2000;16(10-11):1391–1409. https://doi.org/10.1016/S0749-6419(00)00015-2
9. Brüx U., Frommeyer G., Grässel O., Meyer L.W., Weise A. Development and characterization of high strength impact resistant Fe–Mn–(Al, Si) TRIP/TWIP steels. *Steel Research*. 2002;73(6-7):294–298. https://doi.org/10.1002/srin.200200211
10. Frommeyer G., Brüx U., Neumann P. Supra-ductile and high-strength manganese-TRIP/TWIP steels for high energy absorption purposes. *ISIJ International*. 2002;43(3):438–446. https://doi.org/10.2355/isijinternational.43.438
11. Kostina M.V., Bannykh O.A., Blinov V.M. Features of nitrogen-alloyed steels. *Metallovedenie i termicheskaya obrabotka metallov*. 2000;(12):3–6. (In Russ.).

    Костина М.В., Банных О.А., Блинов В.М. Особенности сталей, легированных азотом. *Металловедение и термическая обработка металлов*. 2000;(12):3–6.
12. Mudali U.K., Dayal R.K. Influence of nitrogen addition on the crevice corrosion resistance of nitrogen-bearing austenitic stainless steels. *Journal of Materials Science*. 2000;35(7):1799–1803. https://doi.org/10.1023/A:1004740905317
13. Kostina M.V., Rigina L.G. Nitrogen-containing steels and methods of their production. *Izvestiya. Ferrous Metallurgy*. 2020;63(8):606–622. (In Russ.). https://doi.org/10.17073/0368-0797-2020-8-606-622

    Костина М.В., Ригина Л.Г. Азотосодержащие стали и способы их производства. *Известия вузов. Черная металлургия*. 2020;63(8):606–622. https://doi.org/10.17073/0368-0797-2020-8-606-622
14. Naumenko V.V., Shlyamnev A.P., Filipov G.A. Nitrogen in austenitic stainless steels of various alloying systems. *Metallurg*. 2011;(6):46–53. (In Russ.).

    Науменко В.В., Шлямнев А.П., Филипов Г.А. Азот в аустенитных нержавеющих сталях различных систем легирования. *Металлург*. 2011;(6):46–53.
15. Klotz U.E., Solenthaler C., Ernst P., Uggowitzer P.J., Speidel M.O. Alloy compositions and mechanical properties of 9–12 % chromium steels with martensitic–austenitic microstructure. *Materials Science and Engineering: A*. 1999;272(2):292–299. https://doi.org/10.1016/S0921-5093(99)00490-6
16. Rawers J.C. Characterizing alloy additions to carbon high-nitrogen steel. *Journal of Materials: Design and Applications*. 2004;218(3):239–246. https://doi.org/10.1177/146442070421800309
17. Rawers J.C. Alloying effects on the microstructure and phase stability of Fe–Cr–Mn steels. *Journal of Materials Science*. 2008;43(10):3618–3624. https://doi.org/10.1007/s10853-008-2576-3
18. Mushnikova S.Yu., Kostin S.K., Sagaradze V.V., Kataeva N.V. Structure, properties, and resistance to stress-corrosion cracking of a nitrogen-containing austenitic steel strengthened by thermomechanical treatment. *Physics of Metals and Metallography*. 2017;118(11):1155–1166. https://doi.org/10.1134/S0031918X17110096
19. Scherrer P. Bestimmung der Größe und der inneren Struktur von Kolloidteilchen mittels Röntgenstrahlen. *Nachrichten von der Gesellschaft der Wissenschaften zu Göttingen, Mathematisch-Physikalische Klasse*. 1918;1918(2):98–101. (In Germ.).
20. Timoshenko S.P., Goodier J.N. Theory of Elasticity. New York – Toronto – London: McGraw-Hill book company; 1951:519.
21. Stokes A.R., Wilson A.J.C. The diffraction of X rays by distorted crystal aggregates. *Proceedings of the Physical Society*. 1944:56(3):174–181. https://doi.org/10.1088/0959-5309/56/3/303
22. ASTM G65. Standard Test Method for Measuring Abrasion Using the Dry Sand/Rubber Wheel Apparatus ASTM. 2016:14.

23. Yuan X., Chen L., Zhao Y., Di H., Zhu F. Influence of annealing temperature on mechanical properties and microstructures of a high manganese austenitic steel. *Journal of Materials Processing Technology*. 2015;217:278–285. https://doi.org/10.1016/J.JMATPROTEC.2014.11.027

24. Lee E., Mishra B., Palmer B.R. Effect of heat treatment on wear resistance of Fe–Cr–Mn–C–N high-interstitial stainless steel. *Wear*. 2016;368-369:70–74. https://doi.org/10.1016/j.wear.2016.09.008

25. Speidel M.O. Nitrogen containing austenitic stainless steels. *Materials Science and Engineering Technology*. 2006; 37(10):875–880. https://doi.org/10.1002/mawe.200600068

Information about the Authors

Antonina I. Gordienko, *Cand. Sci. (Eng.), Research Associate of the Laboratory of Physical Mesomechanics and Non-Destructive Control Methods,* Institute of Strength Physics and Materials Science, Siberian Branch of Russian Academy of Sciences
ORCID: 0000-0002-4361-8906
E-mail: mirantil@ispms.ru

Ekaterina V. Abdulmenova, *Cand. Sci. (Eng.), Junior Research of the Laboratory of Molecular Imaging and Photoacoustics,* Institute of Strength Physics and Materials Science, Siberian Branch of Russian Academy of Sciences
ORCID: 0000-0002-9594-5706
E-mail: Ekaterina.V.Abdulmenova@yandex.ru

Tanzilya V. Kozlova, *Cand. Sci. (Phys.-Math.), Junior Research of the Laboratory of Physical Mesomechanics and Non-Destructive Control Methods,* Institute of Strength Physics and Materials Science, Siberian Branch of Russian Academy of Sciences
ORCID: 0000-0003-0890-9983
E-mail: kozlovatv@ispms.ru

Yulia F. Gomorova, *Cand. Sci. (Eng.), Research Associate of the Laboratory of Physical Mesomechanics and Non-Destructive Control Methods,* Institute of Strength Physics and Materials Science, Siberian Branch of Russian Academy of Sciences
ORCID: 0000-0002-0880-2898
E-mail: gomjf@ispms.ru

Il'ya V. Vlasov, *Cand. Sci. (Eng.), Research Associate of the Laboratory of Physical Mesomechanics and Non-Destructive Control Methods,* Institute of Strength Physics and Materials Science, Siberian Branch of Russian Academy of Sciences
ORCID: 0000-0001-9110-8313
E-mail: viv@ispms.ru

Igor' A. Fotin, *Engineer of the Laboratory of Physical Mesomechanics and Non-Destructive Control Methods,* Institute of Strength Physics and Materials Science, Siberian Branch of Russian Academy of Sciences
ORCID: 0000-0001-5185-6405
E-mail: i.fotin2010@gmail.com

Konstantin N. Kayurov, *General Director,* LLK Scientific Production Enterprise of Geophysical "Luch"
ORCID: 0000-0001-9545-5400
E-mail: kayurov@looch.ru

Svetlana P. Buyakova, *Dr. Sci. (Eng.), Prof., Deputy Director for Research, Head of the Laboratory of Physical Mesomechanics and Non-Destructive Control Methods,* Institute of Strength Physics and Materials Science, Siberian Branch of Russian Academy of Sciences
ORCID: 0000-0002-6315-2541
E-mail: sbuyakova@ispms.ru

Сведения об авторах

Антонина Ильдаровна Гордиенко, *к.т.н., научный сотрудник лаборатории физической мезомеханики и неразрушающих методов контроля,* Институт физики прочности и материаловедения Сибирского отделения РАН
ORCID: 0000-0002-4361-8906
E-mail: mirantil@ispms.ru

Екатерина Владимировна Абдульменова, *к.т.н., младший научный сотрудник лаборатории молекулярного имиджинга и фотоакустики,* Институт физики прочности и материаловедения Сибирского отделения РАН
ORCID: 0000-0002-9594-5706
E-mail: Ekaterina.V.Abdulmenova@yandex.ru

Танзиля Вакильевна Козлова, *к.ф.-м.н., младший научный сотрудник лаборатории физической мезомеханики и неразрушающих методов контроля,* Институт физики прочности и материаловедения Сибирского отделения РАН
ORCID: 0000-0003-0890-9983
E-mail: kozlovatv@ispms.ru

Юлия Федоровна Гоморова, *к.т.н., научный сотрудник лаборатории физической мезомеханики и неразрушающих методов контроля,* Институт физики прочности и материаловедения Сибирского отделения РАН
ORCID: 0000-0002-0880-2898
E-mail: gomjf@ispms.ru

Илья Викторович Власов, *к.т.н., научный сотрудник лаборатории физической мезомеханики и неразрушающих методов контроля,* Институт физики прочности и материаловедения Сибирского отделения РАН
ORCID: 0000-0001-9110-8313
E-mail: viv@ispms.ru

Игорь Андреевич Фотин, *инженер лаборатории физической мезомеханики и неразрушающих методов контроля,* Институт физики прочности и материаловедения Сибирского отделения РАН
ORCID: 0000-0001-5185-6405
E-mail: i.fotin2010@gmail.com

Константин Николаевич Каюров, *генеральный директор,* ООО научно-производственное предприятие геофизической аппаратуры «Луч»
ORCID: 0000-0001-9545-5400
E-mail: kayurov@looch.ru

Светлана Петровна Буякова, *д.т.н., профессор, заместитель директора по научной работе, заведующий лабораторией физической мезомеханики и неразрушающих методов контроля,* Институт физики прочности и материаловедения Сибирского отделения РАН
ORCID: 0000-0002-6315-2541
E-mail: sbuyakova@ispms.ru

Contribution of the Authors

A. I. Gordienko – literary review, writing the text, conducting steel quenching, analysis of experimental data.

E. V. Abdulmenova – literary review, writing the text, conducting and analyzing X-ray diffraction studies.

T. V. Kozlova – literary review, writing the text, microhardness measurement, processing results and data analysis.

Yu. F. Gomorova – revision of the text, carrying out structural studies by optical microscopy and the study of fracture surfaces after mechanical testing by scanning electron microscopy.

I. V. Vlasov – carrying out impact bending tests, describing the results of impact tests.

I. A. Fotin – testing of steel samples for abrasive wear, numerical analysis of experimental results.

K. N. Kayurov – formation of the main problem in the field of rotary steerable systems, discussion of the results.

S. P. Buyakova – formation of the main concept, goals and objectives of the study; finalization of the text.

Вклад авторов

А. И. Гордиенко – литературный обзор публикаций по теме статьи, написание текста рукописи, проведение закалки стали, анализ экспериментальных данных.

Е. В. Абдульменова – литературный обзор публикаций по теме статьи, написание текста рукописи, проведение и анализ рентгеноструктурных исследований.

Т. В. Козлова – литературный обзор публикаций по теме статьи, написание текста рукописи, измерение микротвердости, обработка результатов и анализ данных.

Ю. Ф. Гоморова – доработка текста, проведение структурных исследований методами оптической микроскопии, изучение поверхностей изломов образцов после механических испытаний методом растровой электронной микроскопии.

И. В. Власов – проведение испытаний на ударный изгиб, описание результатов ударных испытаний.

И. А. Фотин – проведение испытаний образцов стали на абразивный износ и численный анализ экспериментальных результатов.

К. Н. Каюров – формирование основной проблемы в области роторных управляемых систем, обсуждение полученных результатов.

С. П. Буякова – формирование основной концепции, цели и задач исследования; доработка текста рукописи.

Received 10.10.2023
Revised 01.11.2023
Accepted 10.01.2024

Поступила в редакцию 10.10.2023
После доработки 01.11.2023
Принята к публикации 10.01.2024